Journal of Alloys and Compounds 498 (2010) 13–18

Contents lists available at ScienceDirect

Journal of Alloys and Compounds

journal homepage: www.elsevier.com/locate/jallcom

The magnetic ordering in the Ho_6FeTe_2 compound

A.V. Morozkin[a,*], O. Isnard[b,c], P. Manfrinetti[d,e], A. Provino[d,e], C. Ritter[b], R. Nirmala[f], S.K. Malik[g]

[a] Department of Chemistry, Moscow State University, Leninskie Gory, House 1, Building 3, Moscow GSP-2, 119992, Russia
[b] Institut Laue-Langevin, 6 Rue J. Horowitz, 38042 Grenoble, France
[c] Institut Néel du CNRS - Université J. Fourier, BP166X, 38042 Grenoble, France
[d] Dipartimento di Chimica e Chimica Industriale, Università di Genova, Via Dodecaneso 31, 16146 Genova, Italy
[e] LAMIA Laboratory-CNR-INFM, Corso Perrone 24, 16152 Genova, Italy
[f] Department of Physics, Indian Institute of Technology Madras, Chennai 600 036, India
[g] International Center for Condensed Matter Physics – ICCMP, University of Brasilia, Brasilia 70904-970, Brazil

ARTICLE INFO

Article history:
Received 30 October 2009
Received in revised form 10 March 2010
Accepted 14 March 2010
Available online 19 March 2010

Keywords:
Rare earth intermetallics
Magnetically ordered materials
Neutron diffraction

ABSTRACT

The magnetic structure of the ternary intermetallic compound Ho_6FeTe_2 (hexagonal Zr_6CoAs_2 structure type, a ternary ordered variant of the Fe_2P-type; space group $P\bar{6}2m$, No 189) has been investigated by neutron diffraction and magnetization measurements.

The neutron diffraction study shows that in between the temperatures $T_N \sim 24$ K and $T_C \sim 8$ K the magnetic moments of the Ho atoms adopt a flat helix ordering with elliptical envelope having a wave vector $K = [0, 0, \sim 1/9]$, the helix axis being coincident with the *c*-axis (with maximal magnetic moments of $M_{Ho_1} = 6.5(7)\,\mu_B$ and $M_{Ho_2} = 8.0(7)\,\mu_B$, at 10 K). Below the $T_C \sim 8$ K the magnetic structure of Ho_6FeTe_2 changes to a ferromagnetic cone: superposed on the helix ordering within the basal plane a ferromagnetic ordering with $K = [0, 0, 0]$ and moments pointing in the *c*-direction appears. At 2 K the total maximal magnetic moments amount to $M_{Ho_1} = 9.1(7)\,\mu_B$ and $M_{Ho_2} = 9.6(7)\,\mu_B$ with a ferromagnetic component on the Ho_1 site of $M_{cHo_1} = 2.2(5)\,\mu_B$ and on the HO_2 site of $M_{cHo_2} = 5.2\,(5)\,\mu_B$. No local moment was detected on the iron atomic site in this compound.

Magnetization measurements confirm the first magnetic transition at ~26 K and the second at ~10 K. The magnetization vs. field data obtained at 2.5 K show soft ferromagnetic behavior, with a saturation magnetization of 7.9 μ_B/Ho^{3+}.

1. Introduction

It is known that the series of rare earth intermetallic compounds R_6TA_2 (with R = Gd-Tm; T = Mn, Fe, Co, Ni, Ru and A = Sb, Bi, Te) adopts the hexagonal Zr_6CoAs_2-type structure (space group $P\bar{6}2m$, No 189) [1–4]. This structural prototype is a ternary ordered variant of the Fe_2P structure type [5]. In this crystal lattice the R atoms occupy the 3g and 3f sites, (X_{R1}, 0, 1/2) and (X_{R2}, 0, 0) respectively, the transition metal atoms occupy the special position 1*b* (0, 0, 1/2) and antimony (bismuth, tellurium) atoms occupy the special position 2*c* (1/3, 2/3, 0). From a structural point of view, the Zr_6CoAs_2-type cell of these phases can be regarded as resulting from a double insertion of a p-block element and transition metal atoms into holes of the initial Mg-type rare earth lattice, with corresponding distortion of the starting lattice (Fig. 1). The type of p-element and transition metal 'inserted', and so the level and symmetry of the distortion caused to the Mg-type rare earth sublattice determine the physical properties of the resulting R_6TA_2 compound.

As a rule, the rare earth Zr_6CoAs_2-type compounds demonstrate a commensurate ferromagnetic ordering of the R magnetic moments: either as high-temperature collinear ferromagnets (Tb_6FeBi_2, Ho_6FeSb_2, Ho_6FeBi_2 and Ho_6MnBi_2 $Er_6(Mn,Fe)Sb_2$ and Er_6MnBi_2) or/and as low-temperature non-collinear ferromagnets (Tb_6FeBi_2, Ho_6FeSb_2, Ho_6FeBi_2 and Ho_6MnBi_2) [6–8]. The compound Ho_6CoBi_2 shows high-temperature collinear ferromagnetic ordering, too, but at low-temperature it changes to a ferromagnetic cone with wave vector $K = [0, 0, \pm 1/5]$ [8]. No local moment was detected on the transition metal site. Generally, both the type of transition metal and the distortion of the unit cell strongly affect the ferromagnetic ordering temperature and hence the magnetic structure in these compounds.

To understand the role of transition metal and p-element atoms in the Fe_2P-type R_6TA_2 rare earth systems, the Ho_6FeTe_2 compound was investigated by a neutron diffraction experiment; the results of this work are here reported.

* Corresponding author. Tel.: +7 095 9393472; fax: +7 095 9328846.
E-mail address: morozkin@general.chem.msu.ru (A.V. Morozkin).

0925-8388/$ – see front matter © 2010 Elsevier B.V. All rights reserved.
doi:10.1016/j.jallcom.2010.03.120

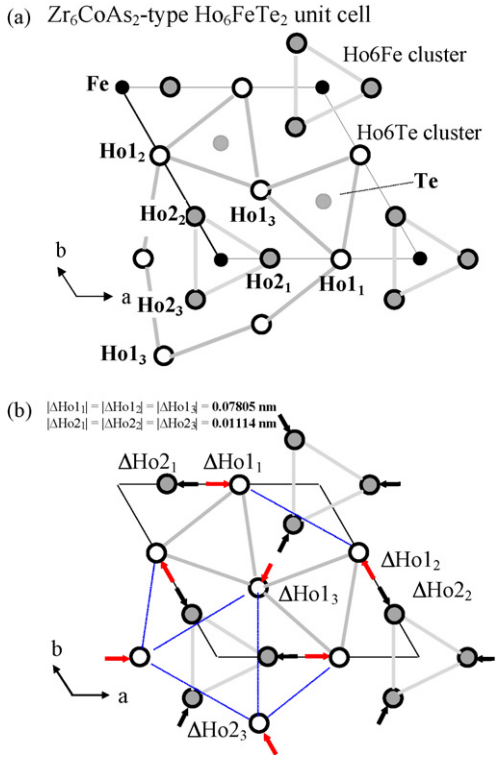

Fig. 1. Hexagonal unit cell of Zr_6CoAs_2-type (Fe_2P-type) Ho_6FeTe_2: (a) distorted Mg-type Ho sublattice in the Fe_2P-type unit cell with set of shifting vectors of the rare-earth atoms from initial site of Mg-type lattice {shifting distances Δ_{Hoij}}, (b) only the final positions of holmium atoms are represented.

2. Experimental details

The alloy was prepared in an electric arc furnace using a non-consumable tungsten electrode, under an argon atmosphere and on a water-cooled copper hearth. Tellurium (purity 99.99 wt.%), holmium (purity 99.9 wt.%) and iron (purity 99.95 wt.%) were used as the starting components. Titanium was used as a getter during melting. Subsequently, the alloy was annealed at 1070 K for 200 h in an argon atmosphere and quenched in ice-water bath. The quality of the sample before the neutron diffraction study was determined using X-ray phase analysis and electron microprobe analysis. The X-ray data were obtained on a diffractometer DRON-3.0 (Cu K_α radiation, $2\theta = 5$–120°, step 0.02°, at 10 s per step). The diffractograms obtained were identified by means of calculated patterns using the Rietan-program [9] in the isotropic approximation. A «Camebax» microanalyser was employed to perform microprobe X-ray spectral analyses of the sample.

The neutron diffraction study was carried out on the powder D1B diffractometer [10] (Institut Laue-Langevin, Grenoble, France), from 58 K down to 2 K (with temperature steps of 2 K). The neutron diffraction patterns were identified and refinements performed using the FULLPROF98-program [11]. A small amount of an unknown impurity phase was detected in the neutron data and the angular regions of its most important Bragg peaks were excluded from the refinements. The coherent scattering length used for the refinement are $0.801 \cdot 10^{-12}$ cm, $0.945 \cdot 10^{-12}$ cm, $0.580 \cdot 10^{-12}$ cm for the Ho, Fe and Te nucleus respectively. To compare with the magnetic structure obtained by neutron diffraction study, dc magnetization was measured in the temperature range of 5 K to 300 K using a commercial magnetometer in fields up to 9 T (Physical Property Measurement System, Quantum Design).

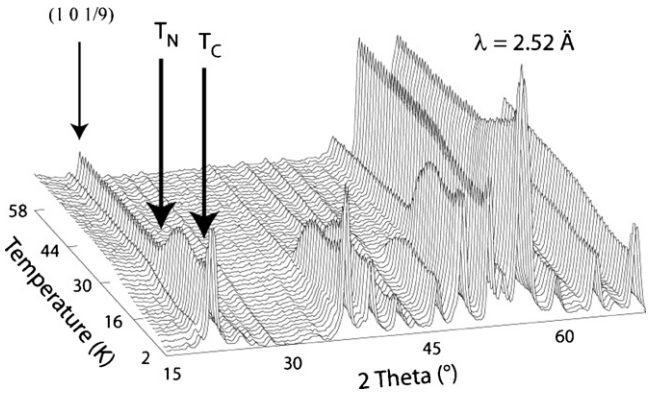

Fig. 2. 3D plot of the thermal variation between 58 K and 2 K of the neutron diffraction patterns of the Ho_6FeTe_2 compound. The lowest 2Θ region has been excluded in the plot due to the very high intensity of the (0, 0, ~1/9) magnetic peak at $2\Theta = 4^\circ$ masking the details of the rest of the figure. At T_N the incommensurate magnetic reflection (1, 0, ~1/9) appears close to the nuclear (1, 0, 0) reflection which itself gains magnetic intensity at T_C.

3. Results and discussion

3.1. Crystal structure

The Mg-type rare earth arrangement can be described in terms of the hexagonal Zr_6FeAs_2-type structure as follows: the rare earth atoms occupy the special positions *3f* (1/3, 0, 0) and *3g* (2/3, 0, 1/2) with the occupation factors for both the transition metal and tellurium (antimony, bismuth) atoms being equal to zero; cell parameters $a = a_{Mg} \cdot (3)^{1/2}$ and $c = c_{Mg}$, space group $P\bar{6}2m$ No 189 ($a = 0.61961$ nm, $c = 0.56158$ nm, $c/a = 0.90635$, $V = 0.18671\ nm^3$ for pure Ho [13]). The presence of the iron and tellurium atoms inserted into the Mg-type rare earth cell leads then to the formation of the Zr_6FeAs_2-type Ho_6FeTe_2 compound ($aHo_6FeTe_2 = 0.81894(4)$ nm, $cHo_6FeTe_2 = 0.39939(2)$nm, X-ray data at 300 K) with a strong distortion of the unit cell [$(aHo_6FeTe_2 - aHo)/aHo = 0.3217$, $(cHo_6FeTe_2 - cHo)/cHo = -0.289$ and $(VHo_6FeTe_2 - VHo)/VHo = 0.2424$].

The lattice of Ho_6FeTe_2 consists of sets of R_6Fe and R_6Te clusters (Fig. 1a). The shortest Ho_1–Te, Ho_1–Ho_2 and Ho_2–Te interatomic distances are close to the sum of the metallic radii of the pure elements ($R_{Ho} = 0.1766$ nm, $R_{Fe} = 0.1241$ nm, $R_{Te} = 0.1432$ nm [12]), whereas the Ho_2–Fe and Ho_2–Ho_2 interatomic distances are less than the sum of metallic radii (Table 1). The holmium atoms occupy the following positions in the unit cell (Fig. 1a):

Ho_1: Ho_{1_1} (xHo_1, 0, 1/2), Ho_{1_2} (0, xHo_1, 1/2), Ho_{1_3} ($-xHo_1$, $-xHo_1$, 1/2);

Table 1
Interatomic distances D in the Ho_6FeTe_2 compounds at 300 K and the ratio δ of D to the sum of the corresponding atomic radii: $\delta = D/(R_{atomic1} + R_{atomic2})$.

Atom1–Atom2	D [nm]	δ	Coordination number	Atom1–Atom2	D [nm]	δ	Coordination number
Ho_1–4Te	0.32005	1.00	13	Fe–$6Ho_2$	0.27939	0.93	11
Ho_1–1Fe	0.32782	1.09		Fe–$3Ho_1$	0.32782	1.09	
Ho_1–$4Ho_2$	0.34853	0.99		Fe–2Fe	0.39939	1.61	
Ho_1–$2Ho_2$	0.35683	1.01					
Ho_1–$2Ho_1$	0.39939	1.13		Te–$3Ho_2$	0.31893	1.00	11
Ho_2–2Fe	0.27939	0.93	14	Te–$6Ho_1$	0.32005	1.00	
Ho_2–2Te	0.31893	1.00		Te–2Te	0.39939	1.39	
Ho_2–$2Ho_2$	0.33844	0.96					
Ho_2–$4Ho_1$	0.34853	0.99					
Ho_2–$2Ho_1$	0.35683	1.01					
Ho_2–$2Ho_2$	0.39939	1.11					

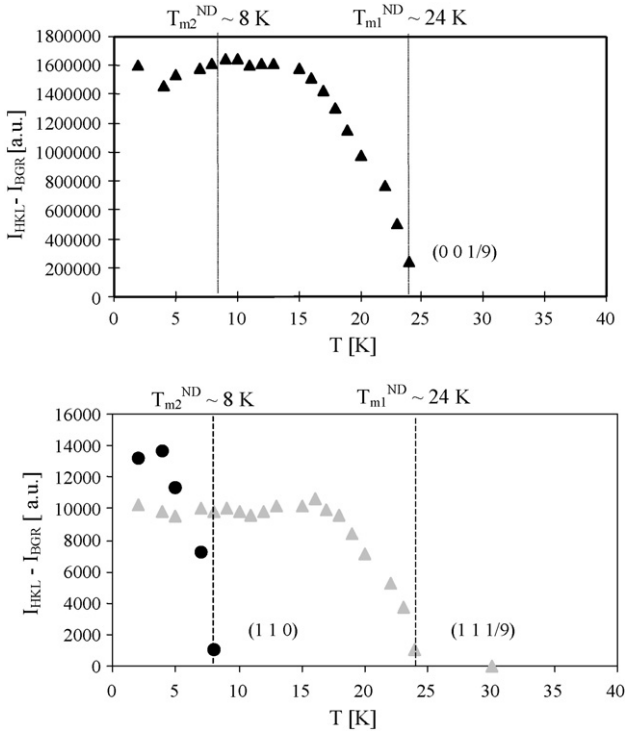

Fig. 3. Thermal variation of the intensity of some of the magnetic reflections of Ho_6FeTe_2.

Ho_2: Ho_{2_1} (x_{Ho_2}, 0, 0), Ho_{2_2} (0, x_{Ho_2}, 0) and Ho_{2_3} ($-xHo_2$, $-xHo_2$, 0).

The free positional parameter was refined from X-ray data at 300 K to $xHo_1 = 0.5997(5)$ and $xHo_2 = 0.2386(5)$. The shifts of the holmium atoms, from their initial positions in the starting Mg-type lattice, are sketched in Fig. 1b.

3.2. Neutron diffraction study

3.2.1. Magnetic transitions

Fig. 2 shows in a 3D plot the thermal variation of the neutron spectra of Ho_6FeTe_2 recorded between 58 K and 2 K. Two transitions are clearly visible which have to be related to the appearance of long-range magnetic order. The low angle region has not been included in Fig. 2 as the intensity of a magnetic peak at $2\Theta \approx 4^\circ$ is extremely strong compared to the other magnetic peaks. The fit of the thermal variation of some of the new magnetic reflections, see Fig. 3, indicates the occurrence of two magnetic ordering temperatures at about 24 K and 8 K in Ho_6FeTe_2.

Fig. 4a shows the neutron diffraction patterns of Ho_6FeTe_2 recorded at 58 K in the paramagnetic phase refined in the space-group *P*-62*m*. The magnetic peaks appearing below 24 K can be indexed with the propagation vector $K = [0, 0, \sim 1/9]$, while below 8 K magnetic reflections with $K = [0, 0, 0]$ e.g. on top of allowed nuclear reflections are as well present.

3.2.2. Magnetic structure

A theoretical analysis of the possible magnetic models for the compounds crystallizing in the Fe_2P structure type was made by Zavorotnev and Medvedeva [13]. The distortion of the initial Mg-type lattice, to obtain the Fe_2P-type unit cell (Fig. 1b), leads to a lowering of the symmetry from D_{6h} down to C_{3v}, destroying the initial collinear order of the rare earth magnetic moments in the *XY* plane. The magnetic structure leading to the upcome of the antiferromagnetic peaks below 24 K can be determined using magnetic symmetry analysis [14,15]. The program BASIREPS included

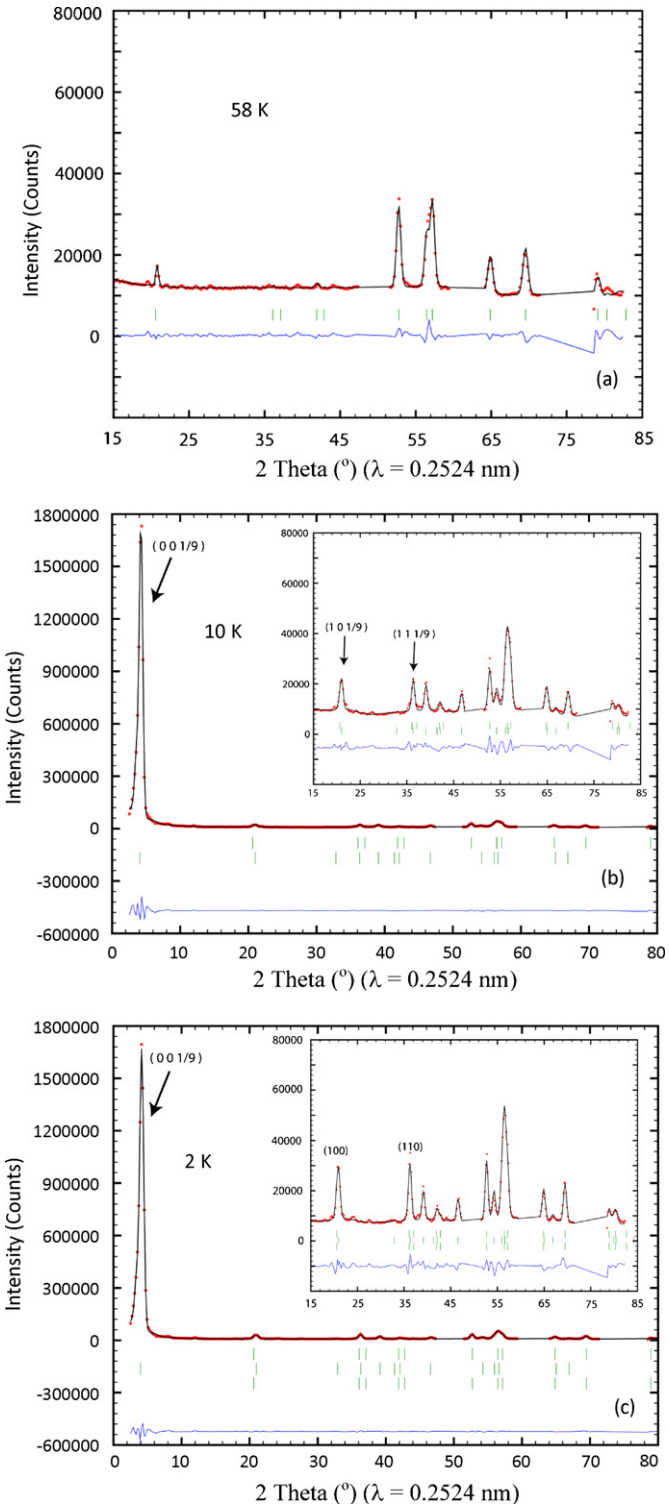

Fig. 4. Neutron diffraction patterns and refinements of the Ho_6FeTe_2 compound: (a) at 58 K (paramagnetic state), (b) at 10 K (antiferromagnetic state) and (c) at 2 K (mixed antiferro-/ferromagnetic state). The refinements show the experimental points (dots) the calculated intensity (line) and their difference (line at the bottom). The vertical bars mark the reflections related to the nuclear and the magnetic phases.

in the FULLPROF suite of programs [11] allows doing this easily by just entering the spacegroup, the propagation vector and the magnetic atom positions. In the case of Ho_6FeTe_2 the symmetry analysis led us to 3 allowed irreducible representations which were tested against the measured neutron diffraction spectra. Table 2 lists the symmetry relations between the 3 different Ho positions

Table 2
Basis vectors of the 3 allowed irreducible representations for $K=[0, 0, \tau]$ and atomic position x, 0, ½ and x, 0, 0. IR = irreducible representation, BV = basis vector, BASR = real part, BASI = imaginary part. IR3 contains altogether 9 BVs which are partly linear combinations of each other, only the first 3 are listed due to space reasons. The refinement of the neutron data made use of BV1 and BV2 of IR3 (marked in bold).

	BV1	BV2	BV3
IR1			
x, y, z			
BASR	1, 2, 0		
BASI	0, 0, 0		
$-y, x-y, z$			
BASR	−2, −1, 0		
BASI	0, 0, 0		
$-x+y, -x, z$			
BASR	1, −1, 0		
BASI	0, 0, 0		
IR2			
x, y, z			
BASR	1, 0, 0	0, 0, 1	
BASI	0, 0, 0	0, 0, 0	
$-y, x-y, z$			
BASR	0, 1, 0	0, 0, 1	
BASI	0, 0, 0	0, 0, 0	
$-x+y, -x, z$			
BASR	−1, −1, 0	0, 0, 1	
BASI	0, 0, 0	0, 0, 0	
IR3			
x, y, z			
BASR	**1, 0, 0**	**0, 1, 0**	0, 0, 1
BASI	**0, 0, 0**	**0, 0, 0**	0, 0, 0
$-y, x-y, z$			
BASR	**0, −0.5, 0**	**0.5, 0.5, 0**	0, 0, −0.5
BASI	**0, −0.866, 0**	**0.866, 0.866, 0**	0, 0, −0.866
$-x+y, -x, z$			
BASR	**0.5, 0.5, 0**	**−0.5, 0, 0**	0, 0, −0.5
BASI	**−0.866, −0.866, 0**	**0.866, 0, 0**	0, 0, 0.866

per site for the 3 allowed representations. Only one out of these 3 possible solutions allows for the magnetic peak intensities. It is a 2-dimensional representation containing real and imaginary components describing with the use of 2 basis vectors (see bold numbers in Table 2) a flat spiral ordering with the spiral axis along the c-axis and the magnetic moment directions within the basal hexagonal plane. Refining the neutron diffraction data at 10 K it turned out that the coefficients of the 2 basis vectors are largely different leading to a strongly elongated envelope of the spiral arrangement. (In the extreme case with one of the coefficients zero a simple spin wave structure results). Due to the overwhelming contribution of the magnetic scattering to the overall scattering the two free atom position parameters were fixed in the low-temperature refinements to the values determined in the paramagnetic state (X-ray data at 300 K and confirmed by neutron data at 58 K). Table 3 contains the refined values of the coefficients of the 2 basis vectors, the resulting maximal magnetic moment values and the refined value of the propagation vector. The magnitude of the magnetic moments on the Ho_1 and Ho_2 sites ($M_{Ho_1} = 6.5(7)\,\mu_B$ and $M_{Ho_2} = 8.0(7)\,\mu_B$) is rather different, with the Ho_2 moments being significantly larger. This is not surprising due to the differing crystallographic surroundings (see below). We have to recall here that the above and further below mentioned magnetic moment values have to be understood due to the strong spin wave like character of the magnetic moments as maximal values. Fig. 4b shows the refinement of the data at 10 K, Fig. 5a and b displays the arrangement of the spins in the unit cell.

Table 3
Refined values of the coefficients $C1$ and $C2$ of the 2 used basis vectors, R_z corresponds to the ferromagnetic component at 2 K in c-direction, M_{max} is the resulting maximal magnetic moment value (see text) and τ the value of the propagation vector in $K=[0, 0, \tau]$. Please recall that $C1$ and $C2$ are not orthogonal to each other but span 120°.

		$C1$	$C2$	F_z	M_{max}	τ
10 K						0.1118 (10)
	Ho_1	7.4 (8)	4.5 (8)	–	6.5 (8)	
	Ho_2	3.1 (9)	9.0 (8)	–	8.0 (7)	
2 K						0.1090 (7)
	Ho_1	10.0 (8)	3.5 (7)	2.2 (5)	9.1 (9)	
	Ho_2	2.3 (8)	9.0 (7)	5.2 (5)	9.6 (8)	

Below 8 K Ho_6FeTe_2 adopts a "mixed" ferromagnetic cone type magnetic structure: while the flat spiral ordering with the propagation vector $K=[0, 0, \sim1/9]$ still persists the increased intensity on top of some of the nuclear peaks indicates the appearance of an additional ferromagnetic coupling. The refinement of the data taken at 2 K was done assuming that both magnetic couplings (antiferromagnetic with $K=[0, 0, \sim1/9]$ and ferromagnetic with $K=[0, 0, 0]$) are embracing the total volume fraction of the sample. The fact that the value of the antiferromagnetic propagation vector changes slightly its value with the upcome of the ferromagnetic compound speaks in favor of this scenario and against a coexistence of two separated magnetic phases as it implies an influence of the ferromagnetic component on the existing antiferromagnetic one. The results of the refinement can be seen in Fig. 4c. Table 3

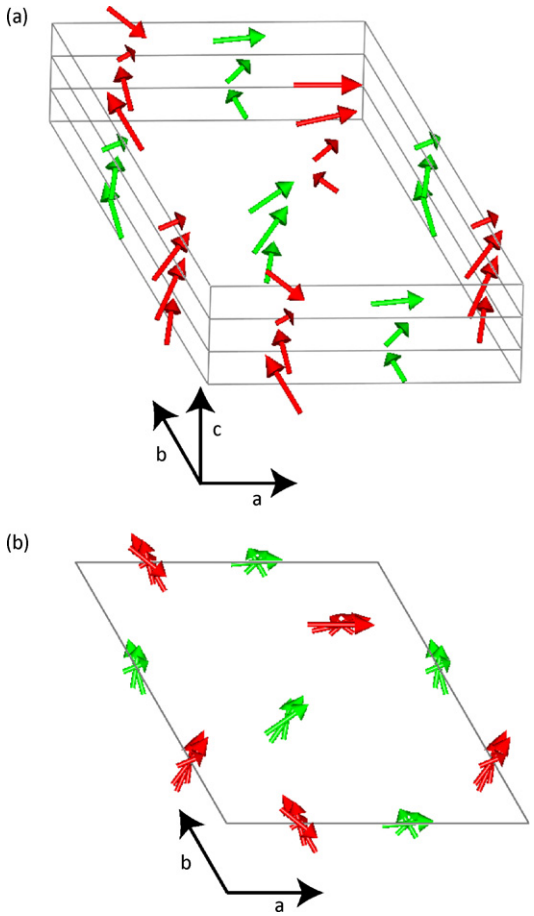

Fig. 5. The magnetic structures of Ho_6FeTe_2. (a) The antiferromagnetic flat spiral structure running along the c-axis with $K=[0,0,\sim1/9]$, (b) projection of the magnetic spins of 3 unit cell onto the basal plane indicating the elliptical envelope of the spiral. (c) The additional ferromagnetic component in c-direction present below 8 K. Ho_1 site spins in green, Ho_2 site spins in red.

contains again the refined values of the propagation vector and of the coefficients of the 2 basis vectors describing the antiferromagnetic coupling, of the ferromagnetic component and the resulting maximal magnetic moment values of the two Ho sites. Amounting to $M_{Ho_1} = 9.1(9)\,\mu_B$ and $M_{Ho_2} = 9.6(8)\,\mu_B$ with a ferromagnetic component on the Ho_1 site of $M_{cHo_1} = 2.2(5)\,\mu_B$ and on the Ho_2 site of $M_{cHo_2} = 5.2\,(5)\,\mu_B$ the maximal magnetic moment values of both sites become more equal and approach within the error bars the theoretical value of the Ho ion in the trivalent state ($M_{Ho^{3+}} = 10\,\mu_B$) [16].

This value is typical of what has been reported earlier from neutron diffraction studies on binary or ternary Ho–Fe intermetallic compounds such as 9 μ_B in Ho_2Fe_{17} [17] or $HoFe_{11}Ti$ [18]. Unlike to these iron rich samples, no ordered 3d magnetic moment is observed in Ho_6FeTe_2. This disappearance of the transition metal magnetism is a rather common feature of rare-earth rich intermetallic compounds and has been attributed to the filling of the 3d band upon hybridization of the rare-earth-transition metal electronic states [19]. The distortion of the initial Mg-type Ho lattice into the final Zr_6CoAs_2-type (Fe_2P-type) Ho_6FeTe_2 compound leads to drastic changes of the magnetic properties of the Ho lattice. While the temperature of the flat spiral ordering decreases from 132 K (Néel point of Ho [16]) down to 24 K for Ho_6FeTe_2 the temperature of the ferromagnetic cone ordering decreases from 20 K (Curie point of Ho [16]) down to 8 K. The wave vector of the Ho lattice changes from K=[0, 0, 1/4.1/5] (Mg-type Ho) to K=[0, 0, ~1/9] (Fe_2P-type Ho_6FeTe_2). While in the initial Mg-type Ho lattice the atoms corresponding to the Ho_1 and Ho_2 sites show the same magnetic behavior, the Ho sublattice in the Fe_2P-type structure is now distorted and consequently the Ho atoms on these two sites are presenting different magnetic moments. This should probably originate from CEF effects which may play a significant role at low-temperature. Indeed the local atomic environment is significantly different for the two inequivalent Ho sites, in particular the Ho_2–Fe distance is shorter than the one observed for the Ho_1 environment. Furthermore the Ho_1 site is surrounded by 13 atoms compared to 14 atoms for Ho_2 site. Neither in the purely antiferromagnetic phase nor in the mixed magnetic phase any indication for a local moment of the transition metal site was found.

3.3. Magnetization studies

To verify the magnetic transition temperatures obtained from the neutron diffraction study, dc magnetization was also measured on a bulk sample of Ho_6FeTe_2 as a function of temperature in applied magnetic field of 0.5 T [Fig. 6]. The dM/dT plot shows two inflection points, one at ~26 K and the other at ~10 K. These temperatures are also marked as peaks in low field magnetization data measured in a field of 0.1 T [see inset of Fig. 6] and agree fairly well with the transition points as obtained from the neutron data. The paramagnetic susceptibility follows a Curie–Weiss behavior with an effective magnetic moment (μ_{eff}) of ~9 μ_B per Ho^{3+} ion and a Weiss temperature of +42 K (θ_p). A small hump visible at about 80 K should be related to the presence of the impurity phase. The hysteresis between the zero-field-cooled and field-cooled magnetization data between 25 K and 9 K is caused by the magnetic structural changes that are occurring in this temperature range. The strong dependence of the magnetization curve on the applied field can be understood from the neutron results as indicating a strong tendency to the induction of the ferromagnetic state at temperatures largely above T_C. The magnetization vs. field data obtained at 2.5 K shows soft ferromagnetic behavior, with a saturation magnetization of 7.9 μ_B/Ho^{3+} (Fig. 7) at 9 T. This is in agreement with the neutron diffraction results where the maximal magnetic moment values of about 9–10 μ_B at 2 K are representing the long axis of the elliptical envelope of the cone (cone = helix + ferromagnetic component) with the short axis being represented by minimal magnetic moment between about 3 μ_B (Ho_1 site) and 5.5 μ_B (Ho_2 site).

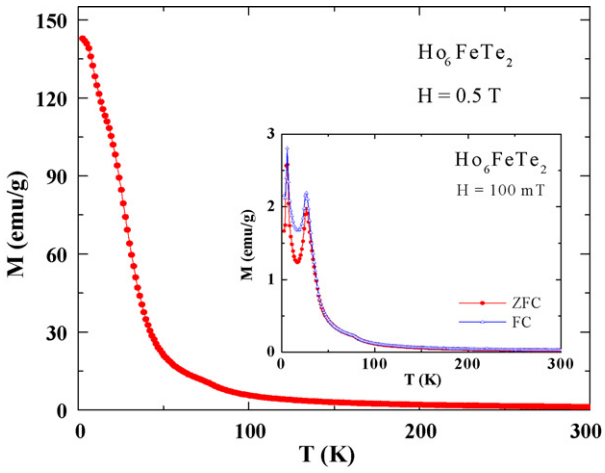

Fig. 6. Temperature (T) variation of magnetization (M) of Ho_6FeTe_2 in an applied field of 0.5 T [in the inset: M vs. T plot, in an applied field of 0.1 T and for the zero-field-cooled (ZFC) and field-cooled (FC) modes].

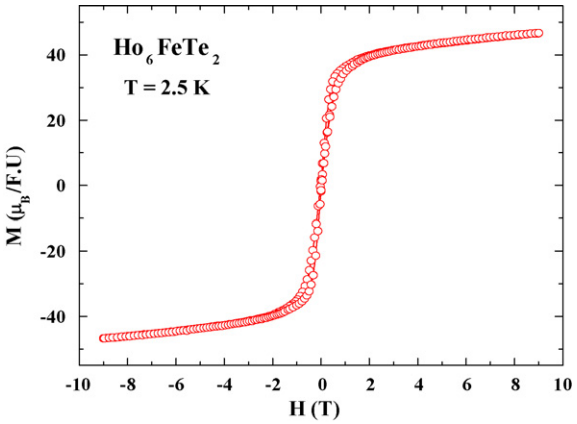

Fig. 7. Magnetization vs. field isotherm obtained at 2.5 K in fields up to 9 T.

4. Conclusion

One can conclude that the distortion of the initial Mg-type Ho lattice in the final Zr_6CoAs_2-type (Fe_2P-type) Ho_6FeTe_2 compound leads to drastic changes of the magnetic properties of the Ho lattice. Although in the intermetallic phase Ho_6FeTe_2 there is a decrease of the magnetic coupling strengths of the Ho lattice with respect to those found in the pure Ho metal, preparation of these Fe_2P-type compounds is a promising way to modify and tune the physical properties of any of the Mg-type rare earths by properly playing on the presence and composition of one or both of the given transition metal or p-block elements, i.e. by preparing mixed-composition alloys such as $R_6(T_{1-x}T'_x)(A_{1-y}A'_y)_2$. Modifications, even subtle, in the crystal structure may lead to interesting changes in the magnetic properties.

Acknowledgments

The present work has received financial support from the *Institut Laue-Langevin*, Grenoble, through the experiment No. 5-31-1908.

This work was supported by the *Russian Fund for Basic Research* through the project No. 09-03-00173-a. This work was supported by the *Indo-Russian Fund for Basic Research* through the project No.

09-03-92653-IND_a. One of the authors, R.N., thanks DST, India, for support received under DST-RFBR program.

This work supported by a ICDD grant no. 05-07. The crystallographic data of Ho_6FeTe_2 used with permission - ©JCPDS - International Centre for Diffraction Data.

References

[1] A.V. Morozkin, J. Alloys Compd. 353 (2003) L16–L18.
[2] A.V. Morozkin, J. Alloys Compd. 358 (2003) L9–L10.
[3] A.V. Morozkin, J. Alloys Compd. 360 (2003) L1–L2.
[4] F. Meng, C. Maliocchi, T. Hughbanks, J. Alloys Compd. 358 (2003) 98–103.
[5] H. Kleinke, J. Alloys Compd. 252 (1997) 29–31.
[6] A.V. Morozkin, V.N. Nikiforov, B. Malaman, J. Alloys Compd. 393 (2005) L6–L9.
[7] A.V. Morozkin, R. Nirmala, S.K. Malik, J. Alloys Compd. 394 (2005) 75–79.
[8] A.V. Morozkin, J. Alloys Compd. 395 (2005) 7–16.
[9] F. Izumi, in: R.A. Young (Ed.), The Rietveld Method, Oxford University Press, Oxford, 1993 (chapter 13).
[10] Yellow Book, at www.ill.fr.
[11] J. Rodriguez-Carvajal, Physica B 192 (1993) 55–69.
[12] J. Emsley, The Elements, second ed., Clarendon press, Oxford, 1991.
[13] Yu.D. Zavorotnev, L.I. Medvedeva, J. Magn. Magn. Mater. 248 (2002) 402–412.
[14] E.F. Bertaut, in: G.T. Rado, H. Shull (Eds.), Magnetism, vol. III, Academic Press, New York, 1963.
[15] Yu.A. Izyumov, V.E. Naish, R.P. Ozerov, Neutron Diffraction of Magnetic Materials, Consultant Bureau, Plenum, NewYork, 1991.
[16] S. Legvold, in: E.P. Wohlfarth (Ed.), Rare Earth Metals and Alloys, Ferromagnetic Materials, vol. 1, North-Holland Publish. Comp., Amsterdam, 1980, pp. 183–295.
[17] O. Isnard, S. Miraglia, J.L. Soubeyroux, D. Fruchart, A. Stergiou, J. Less-Common Metals 162 (1990) 273–284.
[18] R. Apostolov, N. Bezdushnyi, R. Stanev, D. Damianova, J.L. Fruchart, O. Soubeyroux, Isnard, J. Alloys Compd. 265 (1998) 1–5.
[19] E. Burzo, A. Chelkowski, and H. R. Kirchmayr, Magnetic Properties of Metals: Compounds Between Rare Earth Elements and 3d, 4d or 5d Elements, In: H.P.J. Wijn, Landolt-Börnstein, New Series, Group III, vol. 19d2, Springer, Berlin, 1990.